PCCP

View Online
Dynamic Article Links

Cite this: *Phys. Chem. Chem. Phys.*, 2011, **13**, 11294–11302

www.rsc.org/pccp

PAPER

Identification of primary free radicals in trehalose dihydrate single crystals X-irradiated at 10 K†

Mihaela Adeluta Tarpan,‡[a] Hendrik De Cooman,§[ab] Einar Sagstuen,[c] Michel Waroquier[b] and Freddy Callens*[a]

Received 22nd November 2010, Accepted 15th April 2011
DOI: 10.1039/c0cp02616f

Primary free radical formation in trehalose dihydrate single crystals X-irradiated at 10 K was investigated at the same temperature using X-band Electron Paramagnetic Resonance (EPR), Electron Nuclear Double Resonance (ENDOR) and ENDOR-induced EPR (EIE) techniques. The ENDOR results allowed the unambiguous determination of six proton hyperfine coupling (HFC) tensors. Using the EIE technique, these HF interactions were assigned to three different radicals, labeled R1, R2 and R3. The anisotropy of the EPR and EIE spectra indicated that R1 and R2 are alkyl radicals (*i.e.* carbon-centered) and R3 is an alkoxy radical (*i.e.* oxygen-centered). The EPR data also revealed the presence of an additional alkoxy radical species, labeled R4. Molecular modeling using periodic Density Functional Theory (DFT) calculations for simulating experimental data suggests that R1 and R2 are the hydrogen-abstracted alkyl species centered at C5′ and C5, respectively, while the alkoxy radicals R3 and R4 have the unpaired electron localized mainly at O2 and O4′. Interestingly, the DFT study on R4 demonstrates that the trapping of a transferred proton can significantly influence the conformation of a deprotonated cation. Comparison of these results with those obtained from sucrose single crystals X-irradiated at 10 K indicates that the carbon situated next to the ring oxygen and connected to the CH_2OH hydroxymethyl group is a better radical trapping site than other positions.

1. Introduction

Recently, our research groups have engaged in a series of investigations of radiation-induced radicals in sugar derivatives due to their importance with respect to both fundamental and applied research. A number of studies are available that focus on the dosimetric characteristics of sugar systems.[1,2] Other studies, like ours, aim at determining the identity and understanding the structural properties of the radicals involved in the various stages of radiation action. For this purpose, model systems such as glucose,[3,4] sucrose,[5–8] fructose[9–13] and rhamnose[14–17] single crystals have previously been experimentally investigated using Electron Paramagnetic Resonance (EPR), Electron Nuclear Double Resonance (ENDOR) and ENDOR-induced EPR (EIE) spectroscopy, and theoretically by means of Density Functional Theory (DFT) calculations. Next to the relevance of such studies in the context of irradiation of foodstuffs for food preservation and biosecurity,[18] they yield insight in fundamental aspects of direct radiation damage to carbohydrates and, by extension, carbohydrate moieties in biomolecules like DNA. However, one of the most important questions concerning the radiation chemistry of carbohydrates remains: why are certain radicals created after irradiation whereas others, among the large number of possible and likely species, are either not formed or at least to a much lesser extent? Answering this question may allow us to predict *a priori* which radicals will most likely occur in a certain host system. We currently pursue two ways in attempting to understand this selectivity: (i) investigating the plausible reaction mechanisms linking the primary radicals to the stable ones and (ii) studying radical formations in very similar model systems.

The present study focuses on the dominant radicals formed after X-irradiation of trehalose single crystals at 10 K. Firstly, knowledge of these primary radicals is the first step in elucidating reaction mechanisms and can be of great help in identifying the stable radicals obtained after room temperature (RT) X-irradiation, which often have a more extensively altered structure. Secondly, insight into the radiation regioselectivity

[a] *Department of Solid State Sciences, Ghent University, Krijgslaan 281-S1, B-9000 Gent, Belgium. E-mail: Freddy.Callens@ugent.be; Fax: +32 9 264 49 96; Tel: +32 9 264 43 52*
[b] *Center for Molecular Modeling, Ghent University, Technologiepark 903, B-9052 Zwijnaarde, Belgium*
[c] *Department of Physics, University of Oslo, P.O. Box 1048 Blindern, N-0316 Oslo, Norway*

† Electronic supplementary information (ESI) available. See DOI: 10.1039/c0cp02616f

‡ Research assistant of the Fund for Scientific Research—Flanders (F.W.O.—Vlaanderen)

§ Postdoctoral Fellow of the Fund for Scientific Research—Flanders (F.W.O.—Vlaanderen)

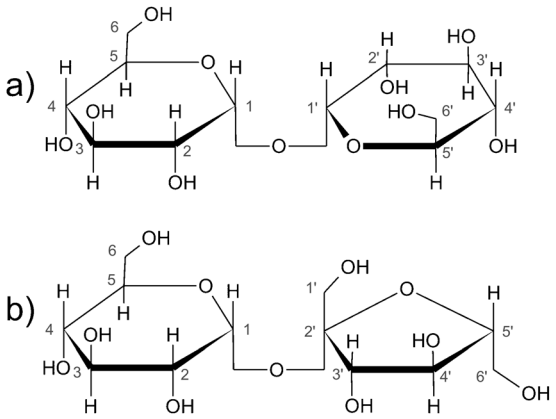

Fig. 1 Chemical structures of trehalose (a) and sucrose (b).

will be obtained by comparing these results with those obtained for sucrose single crystals, which have a close structural similarity (Fig. 1). There are also some major differences between these compounds, most notably the presence of water molecules in crystalline trehalose and the furanosic form of the fructose ring in the sucrose molecule.

Primary radicals trapped in trehalose single crystals X-irradiated at 3 K were previously studied by Samskog *et al.*[19] Three different radicals were identified by EPR: a trapped electron, an alkyl and an alkoxy radical. The alkyl radical was proposed to be a net H-abstracted species centered at either C3 or C3′, while O4′ was suggested as the most probable site of the unpaired electron for the alkoxy radical. The EPR measurements revealed two additional alkoxy radicals for which no hyperfine coupling (HFC) or *g*-tensors were reported.

In the current study, more advanced experimental techniques, like ENDOR and EIE, were used to determine the proton HFC tensors corresponding to the different interactions more accurately. Furthermore, the potential presence of other radical species not easily separable in the EPR spectra but visible in the ENDOR data has carefully been investigated. Periodic DFT calculations have been performed to identify the major radicals and gain insight into their geometric and electronic structure. The present work clearly demonstrates the added value provided by advanced DFT modeling, by highlighting the influence of the radical environment on the radical conformation and electronic properties.

2. Materials and methods

Single crystals of trehalose dihydrate (Sigma–Aldrich) were grown from saturated aqueous solutions containing ethanol by slow evaporation at 10 °C. There are four units of $C_{12}H_{22}O_{11}{\cdot}2H_2O$ in an orthorhombic unit cell ($P2_12_12_1$) with the crystal axes labeled according to the X-ray structure analysis.[20] The unit cell axes were chosen as the reference axes system for the EPR, ENDOR and EIE analysis. The procedures for sample orientation and the EPR/ENDOR/EIE measurements after *in situ* X irradiation at 10 K (to a dose of approximately 45 kGy), using the specially designed setup at the University of Oslo, have been described previously.[11]

The EPR and ENDOR measurements were performed in the *ab*, *bc* and *ca* planes, by rotating the sample in 5° steps over at least 90°. We also performed measurements in a skewed plane ($\theta = 40°$ and $\varphi = 90°$, with θ and φ the usual spherical polar angles) in order to solve the Schonland ambiguity.[21,22] EIE measurements were made with the magnetic field along the crystallographic axes and helped to assign the various ENDOR lines to particular radicals. The proton HFC tensors were determined from the ENDOR angular variations using the MAGRES[23] program. For the determination of the *g* tensors as well as for the simulations of EPR and EIE spectra and of the ENDOR angular variations, the EasySpin[24] routines in Matlab (MathWorks, Inc., Natick, US-MA) were used.

3. Computational details

All calculations were made with the CP2K program package[25] in a periodic approach using the crystal unit cell (containing four trehalose molecules and eight water molecules, 204 atoms in total) as the periodic unit. Geometry optimizations were first made using the Gaussian and plane-waves (GPW) method[26] with a plane-wave cutoff of 320 Ry, TZV2P GTH basis sets[27] and GTH pseudopotentials.[28,29] Subsequently, geometries were further optimized in an all-electron approach using the Gaussian-augmented plane-wave (GAPW) method[30] with a plane-wave cutoff of 250 Ry and TZV2P basis sets. The HFC tensor[31] and ***g***-tensor calculations[32] were also performed using the GAPW method. A BLYP functional[33,34] was employed for all calculations. This method has been validated in similar work on sucrose.[5]

When comparing calculated and experimental eigenvectors or crystal directions, orthorhombic symmetry operations ($x \rightarrow -x$ or $y \rightarrow -y$ or $z \rightarrow -z$) and inversion of eigenvectors were performed on the experimental data to obtain the best possible agreement.

4. Experimental results and radical model assignment

4.1 Experimental EPR, ENDOR and EIE results

All EPR, ENDOR and EIE measurements were carried out at 10 K after *in situ* X-irradiation at 10 K without annealing of the sample between irradiation and measurements. A typical EPR spectrum consists of many strongly overlapping broad resonance lines in the center region (around $g = g_e = 2.0023$; see Fig. 2) together with some weaker lines at either side of the central resonance.

The central part of the X-band EPR spectrum shows only weak anisotropy, typical for alkyl radicals, while the weaker aforementioned resonance lines exhibit fairly anisotropic *g* factors, indicative of alkoxy radicals.[35–37] The HF pattern of the latter signals reveals only rather isotropic HF couplings (HFCs). The *g*-tensor anisotropy was sufficiently small in all cases to allow accurate determination of the HFC tensors from the ENDOR data (see below) assuming isotropic *g*-tensors.

Fig. 3 shows ENDOR spectra recorded for the magnetic field directed along the $\langle a \rangle$-axis. At each orientation of the crystal in the external magnetic field, ENDOR spectra were recorded with the magnetic field locked to at least two different

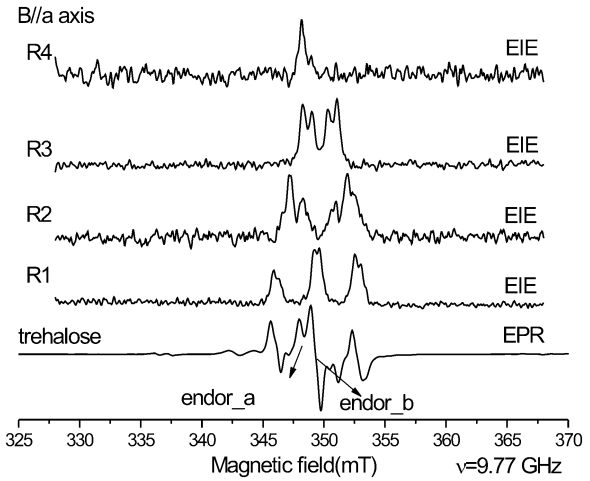

Fig. 2 X-Band EPR (bottom trace, first derivative) and EIE spectra (absorption) of trehalose single crystals X-irradiated at 10 K for the magnetic field along the ⟨*a*⟩ axis. The ENDOR spectra shown in Fig. 3 were obtained with the magnetic field position locked to the EPR lines marked by arrows.

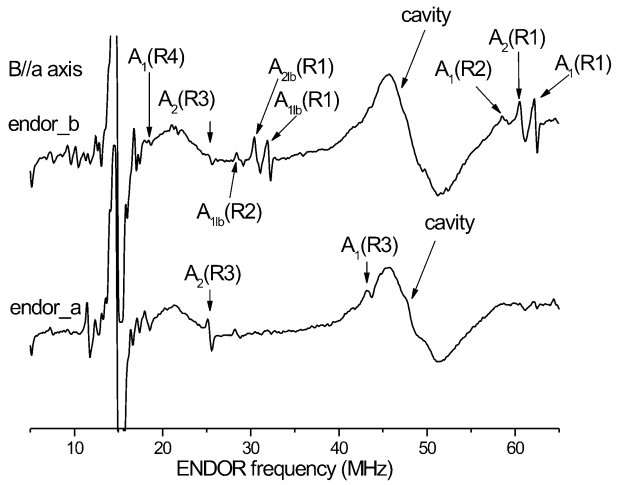

Fig. 3 X-Band ENDOR spectra of trehalose single crystals X-irradiated at 10 K for the magnetic field along the ⟨*a*⟩ axis. The magnetic field was locked at two different positions in the EPR spectrum, as indicated in Fig. 2. "lb" was added to the label of low-frequency ENDOR branches. The broad features at 20–25 and 40–58 MHz (the latter denoted 'cavity') are background detector dc-shifts.

positions in the EPR spectrum. For $B//\langle a\rangle$, the two field positions marked by arrows in Fig. 2 are sufficient to obtain all detectible ENDOR lines. For other orientations, more magnetic field positions had to be selected due to the larger *g*-anisotropy. Six HFC tensors were unambiguously determined from ENDOR angular variations in the three principal crystallographic planes (Fig. 4) and a skewed plane (*cf.* Section 2, not shown here). Even if reliable data from partially deuterated crystals were not obtained in the present work, the anisotropy of the tensors indicates that all six HFCs originate from non-exchangeable positions. Analysis of the EIE spectra shows that they can be attributed to three radicals, labeled R1, R2 and R3 and the corresponding HFC tensors are given in Table 1.

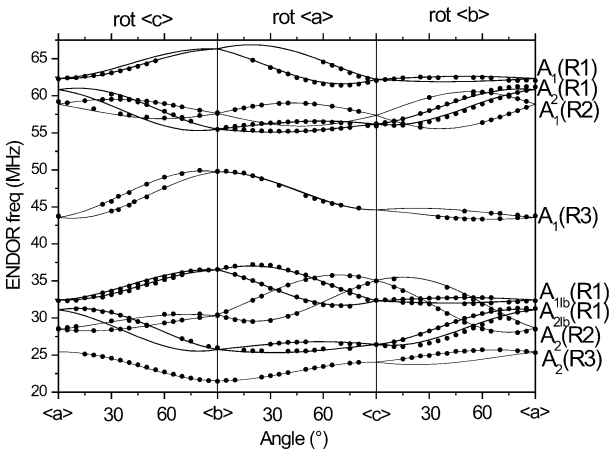

Fig. 4 X-Band ENDOR angular variation in the three principal planes for radical species R1, R2 and R3. The solid circles represent the experimental points for the interactions for which proton HF tensors were determined and the solid lines are simulations using the tensor data in Table 1.

The *g*-anisotropy of the EPR lines assigned to each of the radicals by means of EIE measurements shows that two of the species, R1 and R2, are alkyl radicals, whereas the third one, R3, is an alkoxy radical. Detailed EPR analysis studies revealed the presence of a fourth radical species, R4. The R4 EPR spectra exhibit a relatively large *g*-anisotropy, indicative of an alkoxy radical, and consist of a single line at most orientations. Each of these four radicals will be further discussed in Sections 4.2 and 4.3.

A number of less intense lines exhibiting rather large *g*-anisotropies can be observed in the EPR spectra. These lines could not be assigned because they were not resolved for sufficient orientations of the magnetic field in order to unambiguously determine the corresponding HFC or *g* tensors.

In view of the low temperature used for irradiation and measurements, the radical species discussed in this study may *a priori* be expected to be primary radicals or species closely related to primary radicals. Therefore, structures formed by simple processes like net hydrogen abstractions were inspected first. As will be discussed below, good models were found for R1–R4 considering only such H-abstracted species (R1–R3) or closely related species (R4).

4.2 Alkyl radicals

4.2.1 Radical R1. The EIE spectrum recorded for radical R1 (Fig. 2) is a 1 : 2 : 1 triplet at most orientations and shows that this radical mainly exhibits two fairly isotropic HFCs of about 90 MHz, typical of two (nearly equivalent) β-proton interactions. The HFC tensors are given in Table 1. The presence of a third, small HFC is indicated by an additional, small splitting in the EIE spectrum (triplet of doublets), but sufficient data were not obtained to unambiguously determine the corresponding HFC tensor.

A large number of H-abstracted radicals may exhibit two big and nearly equal β-HFCs in the trehalose molecule: those centered at C2, C3, C4, C5, C2′, C3′, C4′ and C5′. Periodic DFT calculations showed that only the C3-, C4-, C2′-, C3′- and

Table 1 Experimental proton HFC tensors (in MHz) and *g*-tensor obtained from X-band ENDOR and EPR angular variations, respectively, at 10 K for R1, R2 and R3 radicals in trehalose single crystals X-irradiated at 10 K[a]

					Principal directions		
Radical	Tensor	Principal values	A_{iso}	A_{dip}	*a*	*b*	*c*
R1	A_1(R1)	103.92(3)	97.33(3)	6.59(4)	0.033(2)	−0.945(7)	0.326(2)
		95.17(3)		−2.16(4)	0.905(12)	−0.110(8)	−0.411(7)
		92.91(3)		−4.43(4)	0.424(6)	0.308(14)	0.852(2)
	A_2(R1)	92.44(3)	85.23(3)	7.22(4)	0.979(5)	0.171(10)	0.113(6)
		83.38(4)		−1.84(3)	−0.006(9)	−0.527(2)	0.850(17)
		79.85(2)		−5.38(4)	0.205(11)	−0.833(3)	−0.515(3)
R2	A_1(R2)	93.85(2)	86.38(2)	7.47(3)	−0.717(5)	−0.399(9)	0.572(2)
		84.36(2)		−2.02(3)	−0.483(13)	0.876(5)	−0.005(7)
		80.92(3)		−5.45(3)	0.503(10)	0.273(4)	0.820(2)
	A_2(R2)	42.54(6)	32.45(3)	10.09(7)	0.263(9)	0.367(2)	0.892(17)
		28.77(5)		−3.69(6)	0.133(1)	−0.930(4)	0.343(6)
		26.05(4)		−6.40(5)	0.956(12)	0.028(3)	−0.294(9)
R3	A_1(R3)	21.00(3)	17.23(3)	3.77(4)	0.986(7)	0.089(5)	−0.144(5)
		17.63(4)		0.40(4)	0.156(10)	0.148(3)	0.977(4)
		13.05(3)		−4.17(4)	0.065(11)	0.985(13)	−0.159(9)
	A_2(R3)	70.15(2)	62.35(3)	7.80(4)	0.133(14)	−0.991(8)	−0.002(8)
		60.01(3)		−2.34(2)	0.365(3)	0.051(3)	−0.930(7)
		56.90(3)		−5.46(3)	0.922(17)	0.123(6)	0.368(8)
	g	2.0448(1)			−0.041(7)	0.590(12)	0.807(5)
		2.0067(1)			−0.240(5)	−0.789(3)	0.565(11)
		2.0029(2)			0.970(14)	−0.171(2)	0.174(17)

[a] The number in parentheses represents the uncertainty in the last significant digit(s).

C5′-centered radicals exhibit two HF interactions with the required isotropic values of about 90 MHz.

Of these, only the C5′-centered radical (model M1, see Fig. 5) yielded calculated HFC tensors in good agreement with the experimental data (Table 2) with respect to both principal values and principal directions (eigenvectors). This is in particular true for the H′(C6′) tensor where all the eigenvector directions differ by 5° or less from the corresponding experimental results (A_2(R1)). As usual, some discrepancies are encountered for the isotropic values (A_{iso}), but these values are known to be much more sensitive to basis set effects and the level of theory.[38] The periodic DFT calculations also predict the presence of a third, relatively small HFC, H(C6′), with an isotropic value in good agreement with the small HF splitting experimentally observed at some orientations.

The DFT-calculated proton HFC tensors for the H-abstracted C3-, C4-, C2′- and C3′-centered radical models are given in ESI† (Table S1) together with a comparison of the eigenvector directions with the experimental data for radical R1.

Overall, the evidence favoring M1 (net hydrogen abstraction at C5′) as the proper model for radical species R1 is very strong.

4.2.2 Radical R2. The EIE spectrum for radical R2 recorded with the magnetic field along the ⟨*a*⟩-axis is a doublet of doublets (Fig. 2). The HFCs are relatively isotropic (Table 1) indicating that this radical exhibits two β-type proton HF interactions with isotropic couplings of about 90 MHz (A_1(R2)) and 30 MHz (A_2(R2)).

Considering again only net hydrogen abstractions, DFT calculations yielded only two radical models with HFCs of the right magnitude. These C2- and C5-centered radicals are labeled M2 and M3 in Fig. 5. The DFT-calculated proton HF tensors are given in Table 3 together with a comparison with the experimental data of R2.

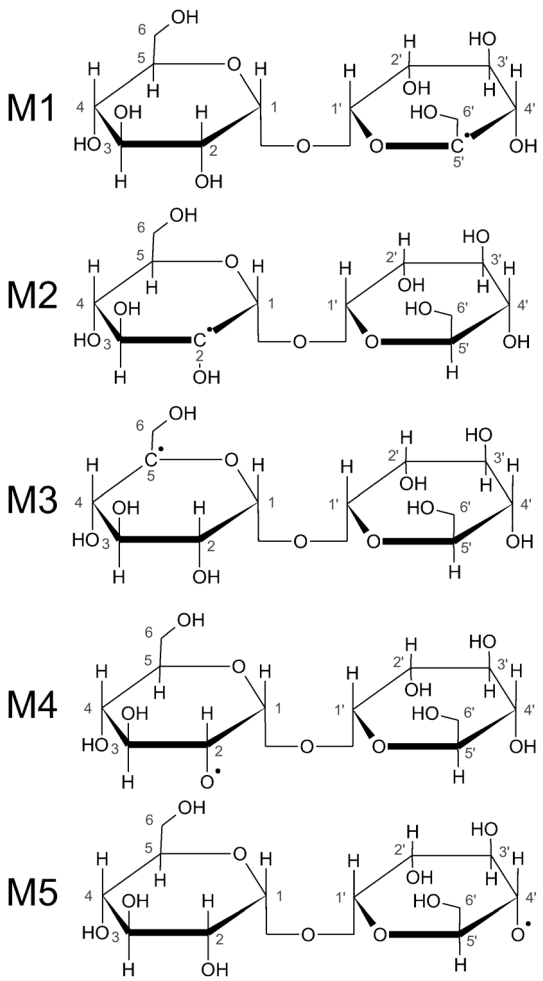

Fig. 5 Chemical structures of the different radical models considered for R1, R2, R3 and R4.

Table 2 DFT-calculated proton HFC tensors (in MHz) for radical model M1 (Fig. 5)[a]

Radical model	Proton	A_{iso}	A_{dip}	Principal directions			δ/°	δ'/°
				a	*b*	*c*		
M1	H(C4′)	89.37	6.72	0.159	−0.980	0.123	14	
			−1.34	−0.845	−0.071	0.531	8	
			−5.38	−0.511	−0.188	−0.839	9	
	H(C6′)	6.04	9.83	−0.589	−0.267	−0.763		
			−3.83	−0.646	−0.412	0.642		
			−6.00	0.486	−0.871	−0.070		
	H′(C6′)	76.67	7.08	0.986	0.092	0.139		5
			−1.95	−0.073	−0.510	0.857		4
			−5.13	0.149	−0.855	−0.496		4

[a] δ and δ' represent the angles between the DFT-calculated and experimental principal directions of A_1(R1) and A_2(R1), respectively.

Table 3 DFT-calculated proton HF tensors (in MHz) for radical models M2 and M3 (Fig. 5)[a]

Radical model	Proton	A_{iso}	A_{dip}	Principal directions			δ/°	δ'/°
				a	*b*	*c*		
M2	H(C1)	12.25	9.47	0.942	0.169	−0.291		55
			−4.12	0.266	−0.903	0.337		8
			−5.35	0.206	0.395	0.895		62
	H(C3)	89.26	6.55	−0.813	0.406	−0.418	10	
			−1.85	0.499	0.855	−0.141	8	
			−4.70	−0.300	0.323	0.898	13	
	H(O2)	0.39	19.59	−0.838	−0.233	−0.493		
			−9.26	−0.418	0.855	0.307		
			−10.34	−0.350	−0.464	0.814		
M3	H(C4)	85.99	7.07	−0.702	−0.432	0.566	2	
			−1.94	−0.538	0.843	−0.024	4	
			−5.13	0.467	0.321	0.824	3	
	H′(C6)	28.26	9.95	0.244	0.347	0.905		2
			−3.50	0.094	−0.938	0.334		2
			−6.46	0.965	0.003	−0.262		2

[a] δ and δ' represent the angles between the DFT-calculated and experimental principal directions of A_1(R2) and A_2(R2), respectively.

The HFC tensors H(C3) and H(C4) from the M2 and M3 radical models, respectively, are very similar to each other and both in good agreement with the experimental A_1(R2) HFC tensor. However, the experimental A_2(R2) tensor is in poor agreement with the calculated H(C1) tensor of model M2 with respect to the principal directions, whereas it fits well with H′(C6) of model M3. Further supported by the very good match in isotropic and anisotropic values (A_{dip}), we conclude that M3 qualifies well as a radical model for R2.

4.3 Alkoxy radicals

4.3.1 Radical R3. Both the EPR and EIE spectra indicate that the HF pattern for R3 is a rather isotropic doublet of doublets that can be explained by the presence of two β- or γ-type HF interactions with isotropic couplings of approximately 62 MHz and 17 MHz. The two HF tensors are reported in Table 1, together with the *g* tensor which was determined from the angular variation of the center of the EPR pattern in the three principal planes (Fig. 6).

An alkoxy radical has its maximum *g* value directed along the C–O bond direction.[39] Therefore, in order to determine plausible sites for the unpaired electron, we compared the eigenvector of the maximum *g*-tensor principal value (g_{max}) with the directions of crystallographic C–O in the pristine molecule (Table 4). Two plausible sites emerge for the unpaired electron: O2 and O4′ (models M4 and M5 in Fig. 5). In Table 5, the DFT calculations for the two radical models are reported and compared with the experimental data.

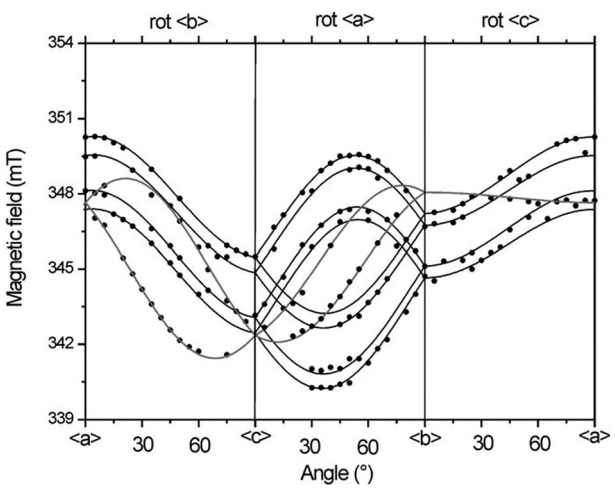

Fig. 6 X-Band EPR angular variation in the three principal planes for R3 (black) and R4 (gray) radicals. The solid circles represent the experimental resonance positions selected from the EPR spectra. The solid lines through the circles are simulations for R3 and R4 using the *g* and HFC tensors reported in Tables 1 and 6, respectively.

Table 4 Angles between the C–O directions in the pristine molecule and the g_{max} principal directions of radicals R3 (δ) and R4 (δ')

	Direction cosines				
	a	*b*	*c*	δ/°	δ'/°
C2–O2	0.037	0.550	0.834	**5**	29
C3–O3	−0.733	−0.348	0.585	45	31
C4–O4	−0.823	0.184	−0.538	54	36
C6–O6	−0.071	−0.946	0.315	72	61
C2′–O2′	−0.826	−0.085	−0.557	64	35
C3′–O3′	−0.292	0.931	−0.221	42	62
C4′–O4′	−0.246	0.373	0.895	**18**	**13**
C6′–O6′	0.313	−0.905	0.287	39	58

Table 6 Experimental *g*-tensor, and estimated A_{max} value (in mT) and corresponding direction cosines of a small proton HFC, for an alkoxy radical in trehalose single crystals irradiated at 3 K, determined from X-band EPR angular variations at 3 K, as reported by Samskog *et al.*[19] This most likely corresponds to radical species R4 in the current study

		Principal values	Principal directions		
Radical	Tensor		*a*	*b*	*c*
R4	*g*	2.0477	−0.347	0.171	0.922
		2.0083	0.586	0.807	0.071
		2.0025	0.732	−0.565	0.380
	A_{max}(R4)	0.7	0.500	0	−0.866

Model M5 can be discarded as it gives rise to a β-proton HF interaction with an isotropic component of more than 100 MHz. The agreement for radical model M4 is, however, good for both the HFC tensors and the *g*-tensor. There is a relatively large deviation between the calculated and experimental g_{max} principal values, but even the current (advanced) methodology is known to be still relatively inaccurate for alkoxy radicals. In conclusion, M4 is a reasonable model for radical R3.

4.3.2 Radical R4. The EIE spectrum of alkoxy radical R4 is a relatively narrow singlet at most orientations. Samskog *et al.*[19] reported the presence of an alkoxy radical at 3 K with the same characteristics (Table 6). The convincing agreement between the simulations with their *g*-tensor with the present experimental angular variation data (Fig. 6) indeed indicates that these two species most likely are the same. Samskog *et al.* also gave a rough estimate of A_{max} (0.7 mT ≈ 20 MHz) and the corresponding principal direction for a small proton HFC (Table 6). It is worth mentioning here that the two 'Schonland conjugate forms' of the *g*-tensor[21,22] are almost identical so that this is not an issue in the discussion below.

The *g*-tensor is typical for an alkoxy radical and the lack of substantial proton HFCs is unusual, but not incompatible with such a radical structure. From a comparison between all crystallographic C–O bond directions and the g_{max} principal direction (see Table 4 and Section 4.3.1), Samskog *et al.* concluded that O4′ is by far the most plausible radical site. However, the DFT-calculated parameters for this model (see M5 in Fig. 5 and 7 and Table 5) differ substantially from the experimental values, most notably: the *g*-tensor principal directions deviate by 24° or more, and as previously mentioned, the H(C4′) proton is predicted to yield an isotropic HFC of

Table 5 DFT-calculated proton HF tensors (in MHz) for radical models M4 and M5 (Fig. 5 and 7)[a]

					Principal directions				
Radical model	Tensor	Principal values	A_{iso}	A_{dip}	*a*	*b*	*c*	δ/°	δ'/°
M4	H(C1)	24.91	20.81	4.10	0.922	0.000	−0.386	15	
		21.00		0.19	−0.386	0.007	−0.922	15	
		16.52		−4.29	−0.003	−1.000	−0.007	10	
	H(C2)	54.73	45.93	8.80	0.009	−0.998	−0.065	8	
		41.76		−4.17	−0.620	−0.057	0.783	17	
		41.30		−4.63	−0.785	0.033	−0.619	18	
	H(C3)	12.67	3.82	8.85	−0.316	0.869	−0.381		
		3.92		0.10	0.514	0.494	0.701		
		−5.14		−8.96	0.797	0.026	−0.603		
	g	2.0302			−0.108	0.642	0.759	6	
		2.0093			−0.395	−0.729	0.559	10	
		2.0031			−0.912	0.239	−0.333	10	
M5	H(C3′)	23.88	13.21	10.67	−0.658	−0.468	0.589		33
		13.22		0.02	−0.572	−0.197	−0.796		
		2.52		−10.69	−0.489	0.861	0.139		
	H(C4′)	116.54	105.15	11.38	−0.316	−0.269	0.910		19
		100.13		−5.02	−0.863	0.481	−0.158		
		98.79		−6.36	0.395	0.835	0.384		
	H(C5′)	4.83	0.26	4.57	−0.024	−0.938	0.345		72
		−1.97		−2.23	0.517	0.284	0.808		
		−2.09		−2.34	−0.856	0.197	0.478		
	H(O6)(Treh2)	14.78	−1.42	16.20	0.205	0.116	0.972		19
		−8.32		−6.90	0.958	0.178	−0.224		
		−10.72		−9.30	0.199	−0.977	0.075		
	g	2.0360			−0.155	0.532	0.833		24
		2.0102			0.034	0.845	−0.533		48
		2.0030			0.987	0.054	0.149		41

[a] δ and δ' represent the angles between the DFT-calculated and experimental principal directions for M4 (δ) and M5 (δ') tensors. For M4, the H(C1) and H(C2) tensors are compared with A_1(R3) and A_2(R3), respectively. For M5, the A_{max} principal directions are compared with the estimated direction of maximum HFC given by Samskog *et al.*[19] (see Table 6).

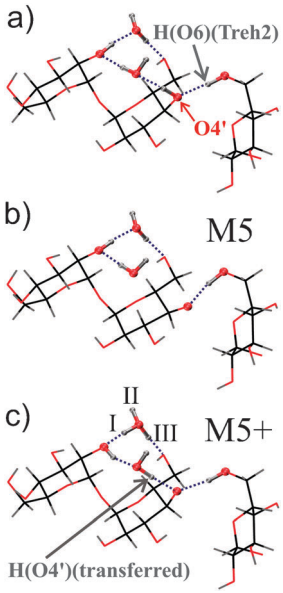

Fig. 7 (a)–(c) DFT-calculated geometries of a trehalose molecule and part of the environment in (a) the pristine lattice, (b) radical model M5, where H(O4′) simply has been removed, and (c) model M5+, where the excess proton has stabilized at a molecule of crystalline water (giving H_3O^+). The dotted lines represent hydrogen bonds. Treh2 is one of the neighboring trehalose molecules.

about 100 MHz. Such discrepancies cannot reasonably be ascribed to an inherent inaccuracy of the DFT-calculated Electron Magnetic Resonance (EMR) parameters.

One possible explanation for this discrepancy is that model M5 is the correct chemical structure for the radical but that it stabilizes in some other geometrical conformation. A plausible trapping mechanism for alkoxy radicals is deprotonation of (excited) cations along hydrogen bonds in the lattice. This separates the spin function from the excess charge, reducing the probability for radical destruction by charge recombination. The presence of the dissociated proton in the neighborhood of the radical and/or an altered hydrogen-bond pattern hence are appealing explanations for possible geometric differences. Searching for alternative minima on the potential energy surface (PES), the O4′·H(O4′) distance for one molecule in a pristine cationic unit cell was first gradually increased (in steps of 10 pm), and geometry optimizations with a constraint on that distance were performed. A semistable configuration (local minimum on the PES) was found with the excess proton bound to a crystalline water molecule, forming a hydronium ion (H_3O^+) three steps down the hydrogen-bond network. An unconstrained optimization of this structure yielded only small geometrical changes and resulted in structure M5+ (Fig. 7c).

The calculated *g*-tensor principal directions of M5+ agree substantially better with the experimental values of R4 (Table 7) than those of M5 (Table 5). Moreover, the isotropic HFC of H(C4′) is strongly reduced: the minor deviation of the A_{max} value (about 14 MHz in the calculations *versus* 20 MHz reported by Samskog *et al.*) now is well within the combined error margin of experiment and calculation. Note that, considering this error margin, the experimentally observed splitting could also originate from the H(C5′) proton ($A_{max} \approx 10$ MHz in the DFT calculation). The A_{max} directions for both the H(C4′) and H(C5′) HFCs differ by about 40° and 60°, respectively, from that reported by Samskog *et al.*, but the experimental uncertainty may be several tens of degrees in this particular case. Also, the calculated g_{max} value is considerably smaller than the experimental one (2.028 *versus* 2.048) but, as commented above already for R3 (Section 4.3.1), this type of discrepancy may well be attributed to the limited accuracy of the DFT *g*-tensor calculations.

Unconstrained reoptimization of the neutral structure obtained by removing either of the three protons (I, II and III in Fig. 7c) of the H_3O^+ molecule in model M5+ results in three semistable configurations (14, 21 and 19 kJ mol^{-1} higher

Table 7 DFT-calculated proton HFC tensors (in MHz) and *g* tensors for radical model M5+ (Fig. 7c)[a]

Radical model	Tensor	Principal values	A_{iso}	A_{dip}	Principal directions			δ/°
					a	*b*	*c*	
M5+	H(C3′)	5.49	1.02	4.46	−0.865	−0.366	−0.342	43
		0.26		−0.76	−0.296	−0.177	0.939	
		−2.68		−3.70	−0.404	0.914	0.045	
	H(C4′)	14.47	6.44	8.03	0.738	0.474	−0.480	38
		2.75		−3.69	0.637	−0.254	0.728	
		2.10		−4.34	−0.223	0.843	0.490	
	H(C5′)	9.43	2.49	6.94	−0.424	−0.831	0.360	58
		1.93		−0.56	−0.662	0.556	0.504	
		−3.89		−6.38	0.618	0.025	0.785	
	H(O6)(Treh2)	11.46	−0.13	11.60	−0.509	−0.496	−0.703	30
		−5.49		−5.35	0.490	−0.839	0.237	
		−6.38		−6.24	−0.708	−0.224	0.670	
	H(O4′) (transferred)	10.92	−0.67	11.59	0.770	0.572	−0.283	51
		−6.26		−5.59	0.632	−0.744	0.217	
		−6.66		−5.99	0.087	0.346	0.934	
	g	2.0286			−0.339	0.069	0.938	6
		2.0112			0.750	0.622	0.225	17
		2.0036			−0.568	0.780	−0.263	17

[a] δ represents the angle between the DFT-calculated and experimental principal directions of the corresponding tensors for radical R4 (Table 6). With respect to HFCs, only a comparison can be made for the A_{max} principal direction.

in energy than M5), with EPR parameters quite comparable to those of M5+ (Table S2 in ESI†). These structures and M5+ have virtually indistinguishable geometries and differ from M5 by a more pronounced tetrahedral configuration of C4′, accompanied by a decrease in spin density at H(C4′), which accounts for the reduced isotropic HFC of H(C4′) in M5+ and its neutral 'derivatives'.

5. Discussion and conclusions

Upon X-irradiation at 10 K, four major radical species (R1–R4) are formed in trehalose dihydrate single crystals. These were all identified as hydrogen-abstracted species: R1 and R2 are alkyl radicals centered at C5′ and C5, respectively, while R3 and R4 are alkoxy radicals, with the spin density mainly at O2 and—most likely—O4′, respectively.

R1 exhibits the same features as the alkyl radical reported in a 3 K irradiation study by Samskog *et al.*,[19] but the present DFT calculations indicate that their radical assignment (centered at C3 or C3′ instead of C5′) is erroneous. R4 most probably is the same radical species as the alkoxy radical reported by Samskog *et al.*[19] Extensive DFT calculations in the present study confirm their assignment of O4′ as a site for the unpaired electron, although the experimental data could not entirely satisfactorily be reproduced. One or more experimental proton HFCs could of course facilitate the identification of R4, but our repeated attempts at extracting them from the ENDOR spectra have so far been unsuccessful. Radical species R2 and R3 have not previously been reported. Conversely, in the present experiments, no strong evidence was found pointing to the presence of the trapped electron, although it was previously claimed to be stable up to 50 K.[19] De Cooman *et al.* faced the same situation for the trapped electron in sucrose single crystals.[7]

The DFT calculations performed for radical R4 provide further evidence that the presence of the abstracted proton, which often is 'ignored' in DFT calculations, may considerably influence the radical conformation, as has previously also been described in sucrose[40] and glucose 1-phosphate.[41] This information, which is only available by advanced periodic DFT modeling, is highly valuable for understanding the oxidative radical trapping mechanism in the solid state and is one example of the added value of using modeling studies in combination with experimental investigations of this type.

Fig. 8 gives an overview of the primary free radicals trapped in sucrose and trehalose single crystals. Although irradiated sucrose was one of the first substances studied in single crystal form by EPR,[42,43] the primary[7] and stable[5,6] radiation products were only recently identified. Using the same methodology as in the current study, four dominant primary species were identified as net H-abstracted radicals in sucrose: three alkyl radical species, centered at C1, C5 and C6 (the latter identification is tentative) and one alkoxy radical, centered at O3′.

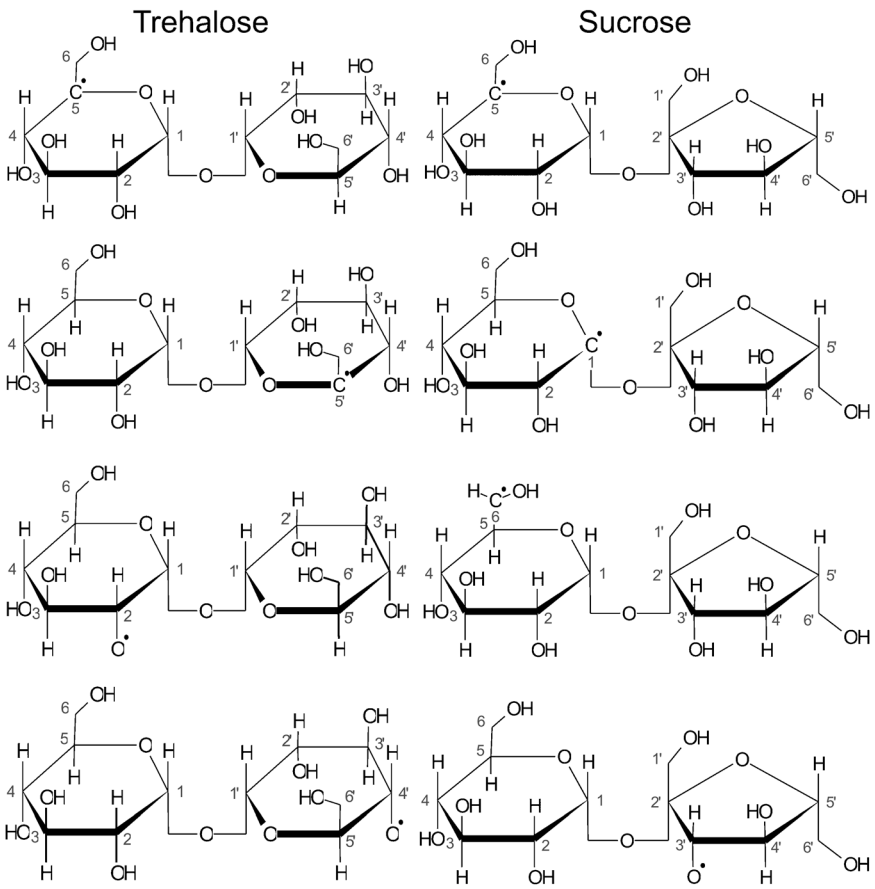

Fig. 8 A summary of the major radical species trapped in 10 K X-irradiated trehalose and sucrose single crystals.

In one of the alkyl radicals in sucrose and both alkyl radicals in trehalose, the radical centre is situated at a carbon situated next to the ring oxygen and connected to the extra-annular hydroxymethyl group. This position thus appears to be a more efficient radical trapping site than other positions. Furthermore, primary species with radical centres at similar positions were previously reported in other carbohydrates, *e.g.* rhamnose,[44] and in the sugar moiety of different nucleosides and nucleotides.[45–48]

Together with the current study, ongoing studies of the stable radicals and radicals obtained in intermediate stages between 10 K and RT in trehalose will allow identifying of the radical processes occurring immediately after irradiation in trehalose and other sugars.

Acknowledgements

The authors wish to acknowledge the Research Foundation-Flanders (Belgium) (F.W.O.-Vlaanderen) and COST P15 for financial support concerning the stay at the University of Oslo. We are grateful for discussions with Prof. Eli O. Hole and excellent technical support from Mr Efim Brondz.

References

1 T. Nakajima, T. Otsuki, H. Hara, Y. Nishiwaki and M. Matsuoka, *Radiat. Prot. Dosim.*, 1990, **34**, 303–306.
2 N. D. Yordanov and R. Mladenova, *Spectrochim. Acta, Part A*, 2004, **60**, 1395–1400.
3 K. P. Madden and W. A. Bernhard, *J. Phys. Chem.*, 1979, **83**, 2643–2649.
4 E. Pauwels, V. Van Speybroeck, G. Vanhaelewyn, F. Callens and M. Waroquier, *Int. J. Quantum Chem.*, 2004, **99**, 102–108.
5 H. De Cooman, E. Pauwels, H. Vrielinck, A. Dimitrova, N. Yordanov, E. Sagstuen, M. Waroquier and F. Callens, *Spectrochim. Acta, Part A*, 2008, **69**, 1372–1383.
6 H. De Cooman, E. Pauwels, H. Vrielinck, E. Sagstuen, F. Callens and M. Waroquier, *J. Phys. Chem. B*, 2008, **112**, 7298–7307.
7 H. De Cooman, E. Pauwels, H. Vrielinck, E. Sagstuen, S. Van Doorslaer, F. Callens and M. Waroquier, *Phys. Chem. Chem. Phys.*, 2009, **11**, 1105–1114.
8 H. De Cooman, E. Pauwels, H. Vrielinck, E. Sagstuen, M. Waroquier and F. Callens, *J. Phys. Chem. B*, 2010, **114**, 666–674.
9 G. Vanhaelewyn, P. Lahorte, F. De Proft, W. Mondelaers, P. Geerlings and F. Callens, *Phys. Chem. Chem. Phys.*, 2001, **3**, 1729–1735.
10 G. C. A. M. Vanhaelewyn, E. Pauwels, F. J. Callens, M. Waroquier, E. Sagstuen and P. F. A. E. Matthys, *J. Phys. Chem. A*, 2006, **110**, 2147–2156.
11 M. Tarpan, E. Sagstuen, E. Pauwels, H. Vrielinck, M. Waroquier and F. Callens, *J. Phys. Chem. A*, 2008, **112**, 3898–3905.
12 M. A. Tarpan, H. Vrielinck, H. De Cooman and F. Callens, *J. Phys. Chem. A*, 2009, **113**, 7994–8000.
13 M. A. Tarpan, E. Pauwels, H. Vrielinck, M. Waroquier and F. Callens, *J. Phys. Chem. A*, 2010, **114**, 12417–12426.
14 P. O. Samskog, L. D. Kispert and A. Lund, *J. Chem. Phys.*, 1983, **79**, 635–638.
15 P. O. Samskog, A. Lund, G. Nilsson and M. C. R. Symons, *J. Chem. Phys.*, 1980, **73**, 4862–4866.
16 P. O. Samskog and A. Lund, *Chem. Phys. Lett.*, 1980, **75**, 525–527.
17 H. C. Box, E. E. Budzinski and H. G. Freund, *Radiat. Res.*, 1990, **121**, 262–266.
18 J. F. Diehl, *Safety of Irradiated Foods*, Marcel Dekker, New York, 1995.
19 P. O. Samskog, L. D. Kispert and A. Lund, *J. Chem. Phys.*, 1983, **78**, 5790–5794.
20 G. M. Brown, D. C. Rohrer, B. Berking, C. A. Beevers, R. O. Gould and R. Simpson, *Acta Crystallogr., Sect. B: Struct. Crystallogr. Cryst. Chem.*, 1972, **28**, 3145–3158.
21 D. S. Schonland, *Proc. Phys. Soc.*, 1959, **73**, 788–792.
22 H. Vrielinck, H. De Cooman, M. A. Tarpan, E. Sagstuen, M. Waroquier and F. Callers, *J. Magn. Reson.*, 2008, **195**, 196–205.
23 W. H. Nelson, *J. Magn. Reson.*, 1980, **38**, 71–78.
24 S. Stoll and A. Schweiger, *J. Magn. Reson.*, 2006, **178**, 42–55.
25 http://cp2k.berlios.de.
26 G. Lippert, J. Hutter and M. Parrinello, *Mol. Phys.*, 1997, **92**, 477–487.
27 G. Lippert, J. Hutter, P. Ballone and M. Parrinello, *J. Phys. Chem.*, 1996, **100**, 6231–6235.
28 S. Goedecker, M. Teter and J. Hutter, *Phys. Rev. B: Condens. Matter*, 1996, **54**, 1703–1710.
29 C. Hartwigsen, S. Goedecker and J. Hutter, *Phys. Rev. B: Condens. Matter Mater. Phys.*, 1998, **58**, 3641–3662.
30 G. H. Lippert, J. Hutter and M. Parrinello, *Theor. Chem. Acc.*, 1999, **103**, 124–140.
31 R. Declerck, V. Van Speybroeck and M. Waroquier, *Phys. Rev. B: Condens. Matter Mater. Phys.*, 2006, **73**, 115113.
32 V. Weber, M. Iannuzzi, S. Giani, J. Hutter, R. Declerck and M. Waroquier, *J. Chem. Phys.*, 2009, **131**, 14106–14117.
33 A. D. Becke, *Phys. Rev. A: At., Mol., Opt. Phys.*, 1988, **38**, 3098–3100.
34 C. T. Lee, W. T. Yang and R. G. Parr, *Phys. Rev. B: Condens. Matter*, 1988, **37**, 785–789.
35 S. E. Locher and H. C. Box, *J. Chem. Phys.*, 1980, **72**, 828–832.
36 E. E. Budzinski, W. R. Potter and H. C. Box, *J. Chem. Phys.*, 1980, **72**, 972–975.
37 K. P. Madden and W. A. Bernhard, *J. Chem. Phys.*, 1979, **70**, 2431–2437.
38 R. Improta and V. Barone, *Chem. Rev.*, 2004, **104**, 1231–1253.
39 W. A. Bernhard, D. M. Close, J. Huttermann and H. Zehner, *J. Chem. Phys.*, 1977, **67**, 1211–1219.
40 H. C. Box and E. E. Budzinski, *J. Chem. Phys.*, 1983, **79**, 4142–4145.
41 E. Pauwels, H. De Cooman, G. Vanhaelewyn, E. Sagstuen, F. Callens and M. Waroquier, *J. Phys. Chem. B*, 2008, **112**, 15054–15063.
42 H. Ueda, Z. Kuri and S. Shida, *J. Chem. Phys.*, 1961, **35**, 2145.
43 H. Shields and P. Hamrick, *J. Chem. Phys.*, 1962, **37**, 202–203.
44 E. Sagstuen, M. Lindgren and A. Lund, *Radiat. Res.*, 1991, **128**, 235–242.
45 K. P. Madden and W. A. Bernhard, *J. Phys. Chem.*, 1980, **84**, 1712–1717.
46 E. O. Hole, W. H. Nelson, E. Sagstuen and D. M. Close, *Radiat. Res.*, 1992, **130**, 148–159.
47 W. H. Nelson, E. Sagstuen, E. O. Hole and D. M. Close, *Radiat. Res.*, 1998, **149**, 75–86.
48 E. O. Hole, E. Sagstuen, W. H. Nelson and D. M. Close, *Radiat. Res.*, 2000, **153**, 823–834.

